SOURIS

Stanford One Unit Rocket In Space

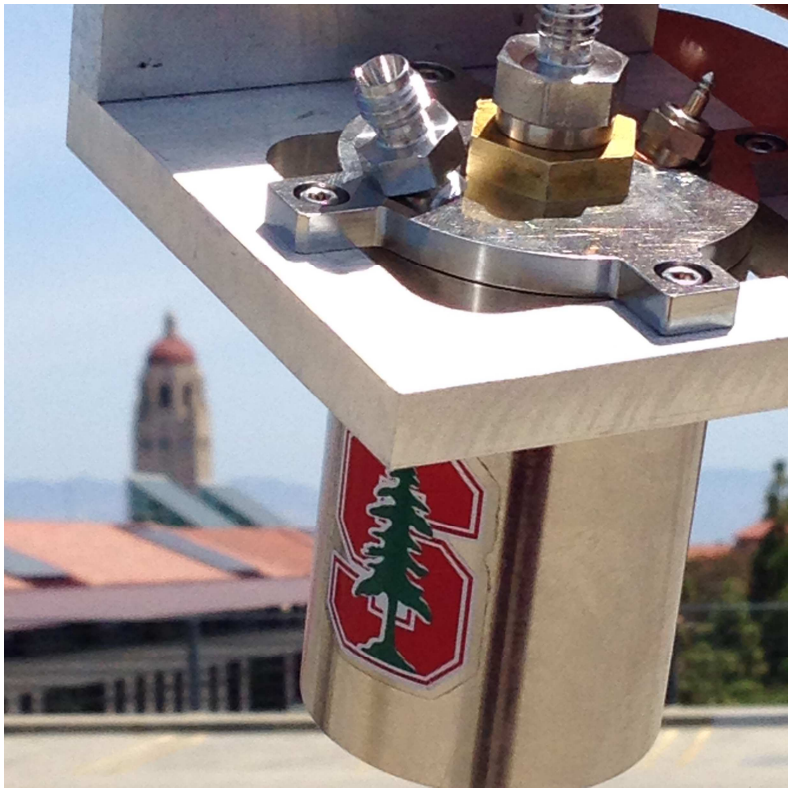

AA284

2013-2014

SUMMARY

This report presents the design, manufacturing and testing of a hybrid propulsion system for a CubeSat using Nitrous Oxide and PMMA. This project was conducted at Stanford University, in the AA284 (Advanced Rocket Propulsion) series.

D. Asturias, P. Desai, F. Mechentel, M. Nations, JP. Shivanandan, G. Sugar, B. Todd

STANFORD AERONAUTICS & ASTRONAUTICS

LELAND STANFORD JUNIOR UNIVERSITY DIE LUFT DER FREIHEIT WEHT 1891

SPaSE

Introduction

In recent years, CubeSats have given many universities and organizations the ability to conduct space-based experiments for a reasonable price. Unfortunately, the orbits of these satellites are limited because they are launched as secondary payload and the options for a propulsion system on this scale are limited. The growth and potential of the CubeSat industry has dictated the need for a propulsion system that meets the CubeSat standards and can be readily obtained. To address this need, the development of a hybrid based propulsion system was carried out to determine the capabilities of hybrid rockets for use with CubeSats.

A few systems have already been designed for CubeSat applications, such as the MRS-142 CubeSat High-impulse Adaptable Monopropellant Propulsion System (CHAMPS). The engine is documented to produce a total impulse of 800 N.s and fits in a 1U configuration. However, this system uses hydrazine, which should be phased out of the space industry due to environmental regulations and handling hazards. As a result, to better supply the needs of the CubeSat industry, a propulsion system which can be contained within a single unit and use non-hazardous fuels was designed.

CubeSat Hybrid Propulsion Design

Design requirements

While it would be desirable to keep the weight of the system within CubeSat standards for 1U (1.3 kg/U), this is not likely possible and thus a soft requirement was placed on the weight of the system fully loaded to be equal or less than 1.3 kg.

In terms of the propulsion system performance characteristics, the system was designed to be greater than the industry mean for cold gas thrusters, about 160 Ns. The maximum allowable thrust output of the system was set to 20 N to keep acceleration rates low for the internal components. The total power required for the system was to not exceed 10 W during operation and 5 W for startup and system checks. The system is non-restart able to reduce complexity. From these requirements, a 1U system was designed and manufactured within a budget of $15,000. The prototype was placed under a number of tests to verify the analysis work and performance metrics. The final requirements are presented below.

Design requirements	
Tank Temperature	20° C, 293 K
Tank Pressure	733 psi
Total Oxidizer Mass	200 g
Vapor Mass Fraction	12.5 %
Average Chamber Pressure	270 psi
Burn time	45 s
Average Thrust	11 N
Max Thrust	13.25 N
Average vacuum I_{sp}	300 s
Total Impulse	495 N.s

Table 1: Design requirements.

Fuel Selection

To meet the low thrust requirement it is desirable to have an average fuel regression rate to be relatively low and the expected average oxidizer mass flow was selected to be around 5 g/s. From a previous study by a similar Stanford project on low regression rate fuels, three fuel types of solid fuels were considered: PMMA, HTPB and HDPE. These provided the lowest regression rates based on the expected oxidizer mass flux rates. Additionally, two oxidizers were selected: N_2O and H_2O_2. However, N_2O was ultimately selected for its density and it is less hazardous than the H_2O_2.

The following chart shows the sizing study performed with each of the solid fuel grains with N_2O. For the most part, all of the fuel grains can achieve the same vacuum I_{sp} performance under the optimal O/F ratios. However, when analyzing the required fuel grain size, there are two distinct geometries that emerge: a short and wide or long and thin grain. From the geometry constraints, this can greatly affect the other components and will affect the mass of the system. Additionally, the overall system density of each of the fuels were 1.622 g/cm^3 for PMMA, 1.632 g/cm^3 for HDPE and 1.635 g/cm^3 for HTPB. As a result, PMMA appeared to be the best option for designing a thrust chamber that would minimize the size requirements for the given weight and required a long skinny chamber in the center of the CubeSat unit.

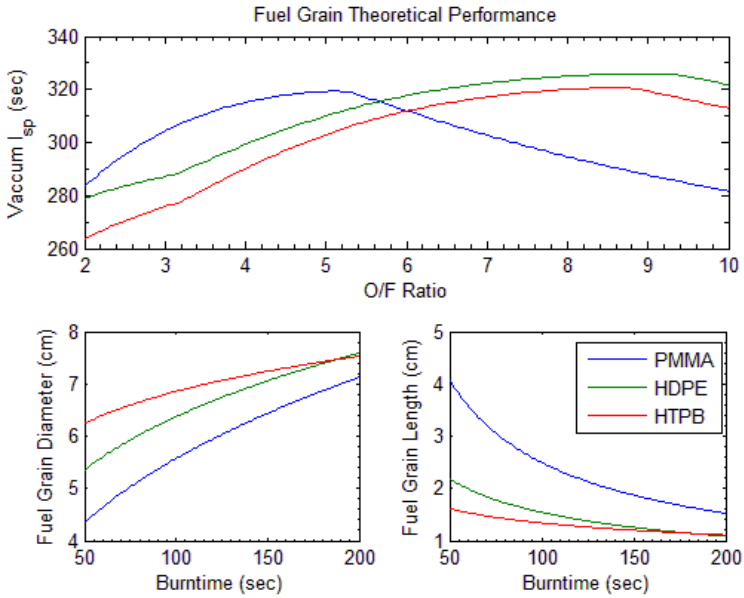

Figure 1: Fuel grain theoretical performance.

Thrust Chamber Design

From the selected fuel grain geometry a chamber was designed to contain the combustion process. To maintain combustion during the burn and prevent fire blowdown events, a microscopic orifice was fashioned at the entrance of the thrust chamber. To start the combustion process, a glow plug with a black powder variant would provide the ignition energy required for the sustained

combustion. To protect the top plate from the temperatures within the chamber, a garolite[1] insert was positioned between the fuel grain and steel. To monitor the chamber pressure, a small pressure port was made on the top of the thrust chamber plate. Due to the long burn time, a solid graphite insert could not be used for the nozzle geometry as it would transfer too much heat to the chamber walls. As a result, a graphite nozzle surrounded in garolite would provide the required outlet geometry while protecting the combustion chamber walls.

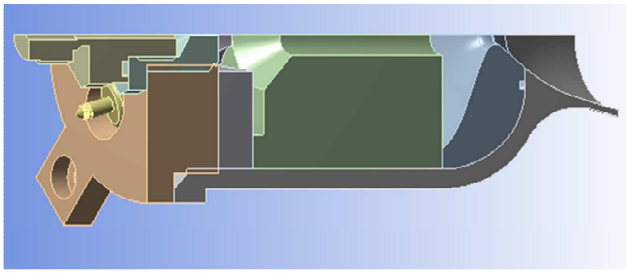

Figure 2: 3D cross-section of the combustion chamber.

Tank Design

With a thrust chamber designed, the oxidizer tank needed to be designed around the chamber such that it could hold the required amount of oxidizer and the thrust was directed along the center line of the CubeSat. Thus, a torodial tank was the only solution to house the N_2O propellant and fit within the single CubeSat unit. However, a standard circular torodial tank would not meet the storage requirements and a more rectangular tank needed to be used to hold the oxidizer. From an initial structural analysis, the exterior walls had large deformations and bending stresses that would be unacceptable for the CubeSat. Thus, internal stiffeners were added to relieve some of the stress and deflection. The pictures below show a full 3D CAD of the tank geometry as well as a half symmetry model of the tank from finite element analysis to understand the stress fields within the tank.

[1] G10 Garolite, high performance fiberglass composite material

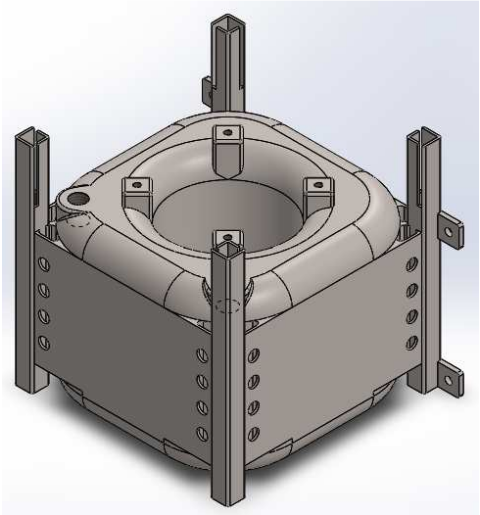

Figure 3: 3D CAD model of the oxidizer tank.

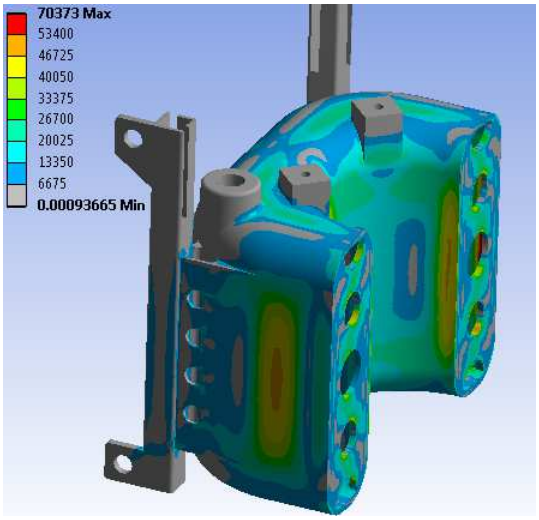

Figure 4: Structural analysis of the oxidizer tank.

This creates a complicated geometry around the thrust chamber, which cannot be machined by traditional means, but could be 3D printed. Aluminum, stainless steel and titanium were considered, but the thickness required to hold the maximum expected operating pressure had a large impact on the weight and internal volume of the tank. Using factors of safety of 2.0 on yield and 2.5 on ultimate, the required dimensions and weight of the aluminum and stainless steel tanks exceeded the requirements. As a result, Titanium 6Al-4V was the only material that could meet all of the requirements due to its favorable strength to density ratio. Additional support structure was added to the exterior of the tank to provide the rail system for the PPOD system and additional hold locations for testing.

Predicted Performance

With the designed system, a time iteration scheme was developed to determine the time history of critical components during the burn. The blowdown of the oxidizer tank is simulated using an equilibrium model presented in "Review and Evaluation of Models for Self-Pressurizing Propellant Tank Dynamics"[2] which assumes that all the propellant in the tank remains in phase equilibrium. The model provides us with a fair estimation of the pressure drop in the tank with time as long as the flow out of the tank can be considered slow compared to the heat and mass transfer between the liquid and vapor. The heat transfer rate used in the energy equation was iteratively determined in order to have a 10-15° temperature drop in the tank, as seen in previous data. A reasonable value was found to be -700 W. A block diagram representing the structure of the code is presented below.

[2] Zimmerman, J. E., Waxman, B. S., Cantwell, B. J., and Zilliac, G. G., "Review and Evaluation of Models for Self-Pressurizing Propellant Tank Dynamics", 49th AIAA/ASME/SAE/ASEE Joint Propulsion Conference, San Jose, CA, 2013

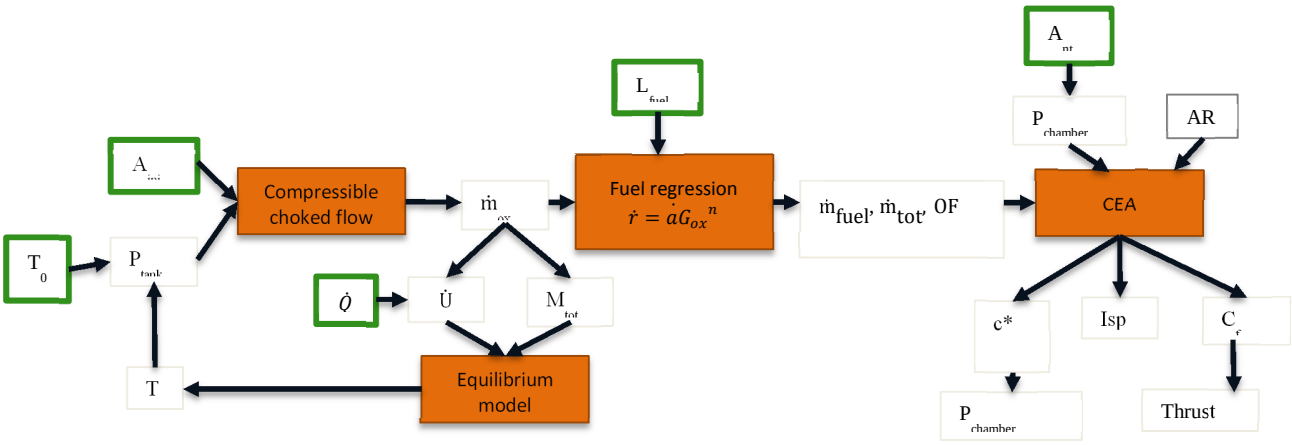

Figure 5: Structure of the simulation code.

The charts below show the time dependency of particular parameters of interest within the propellant tank and the thrust chamber using this model.

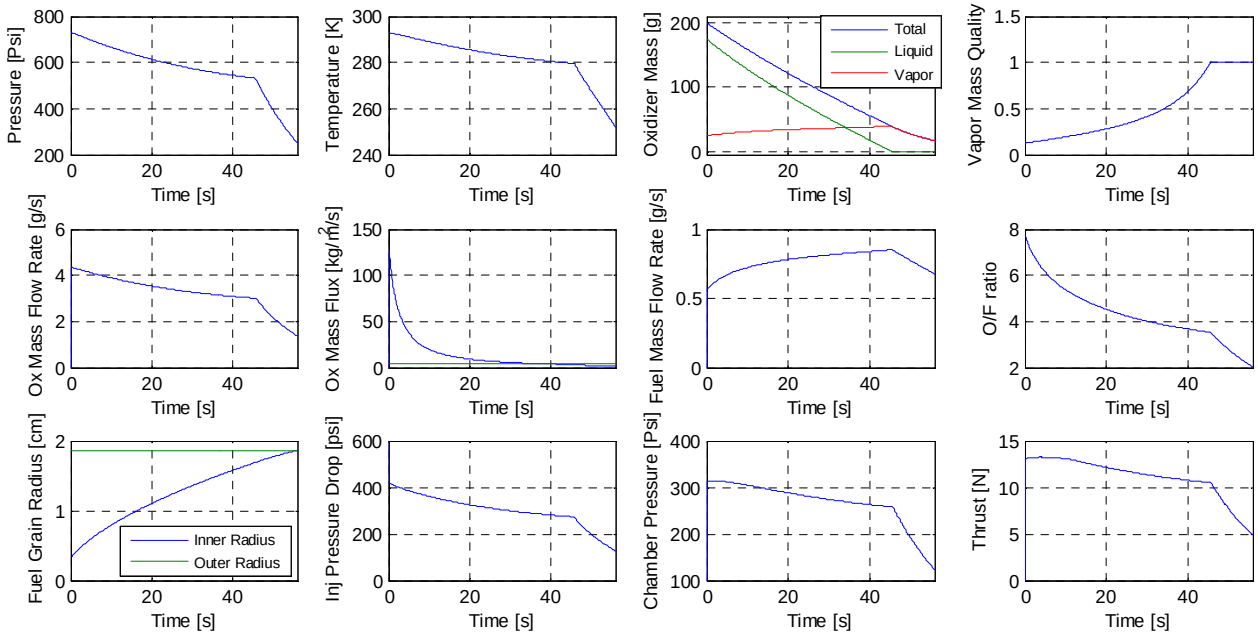

Figure 6: Engine parameters time histories.

The curve changes from a quasi linear decay to an exponential decay when the oxidizer in the tank is gaseous. This transition can be seen on the “Oxidizer Mass” plot and the “Vapor Mass Quality”. In this model, constant port regression with length is assumed and thus, analysis of the “Fuel Grain Radius” plot limits the burn time. Note the wide O/F shift, due to the significant decrease in oxidizer mass flow rate during the burn. The average thrust in vacuum is 11N.

Prototype

With a finalized design, the components were manufactured by local vendors. Most of the components arrived to specification. However, there was a great deal of difficulty with the 3D printing process used for the tank geometry and none of three titanium tanks manufactured were useable. All the tanks had a printing imperfection which caused it to leak under no pressure and were unusable due to buildups and cavities of material on the upper surface. It was determined the curves on the top side of the tank were too complicated for the machines to replicate reliably. However, a completed system without feedlines was assembled and weighed for a dry mass of 1.2118 kg and an estimated wet mass of 1.42 kg.

Testing

Pressure and Compatibility Testing of the Tank

During the time of the manufacturing, there was limited experience with titanium printing and many companies were not willing to print the desired design. One company was found that believed it could print the tank to the desired specifications. However, the company attempted to print the tank three times to no success and some of the printing flaws encountered can be viewed below. Most of these flaws are attributed to an unsteady shaving spreader which would leave voids and large deposits on certain surfaces. Additionally, it appears that the laser was not correctly tuned in some locations and the sintering did not leave a good connection. After these three failed printing attempts, the company manufactured a stainless steel version with some flaws which were welded post printing process. While this is not a viable option for a space mission, this tank will be used for hydrostatic testing to validate the structural analysis of the design.

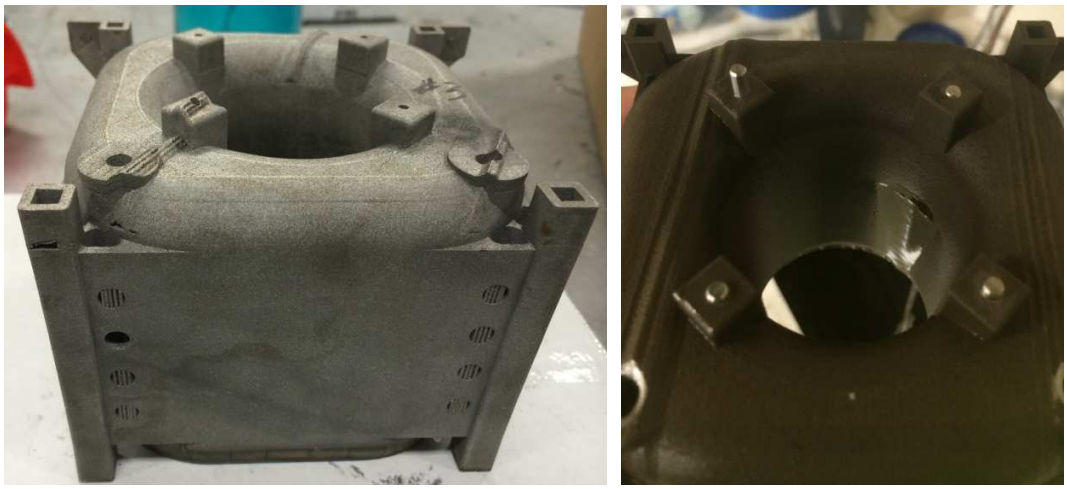

Figure 7: 3D printed titanium tank.

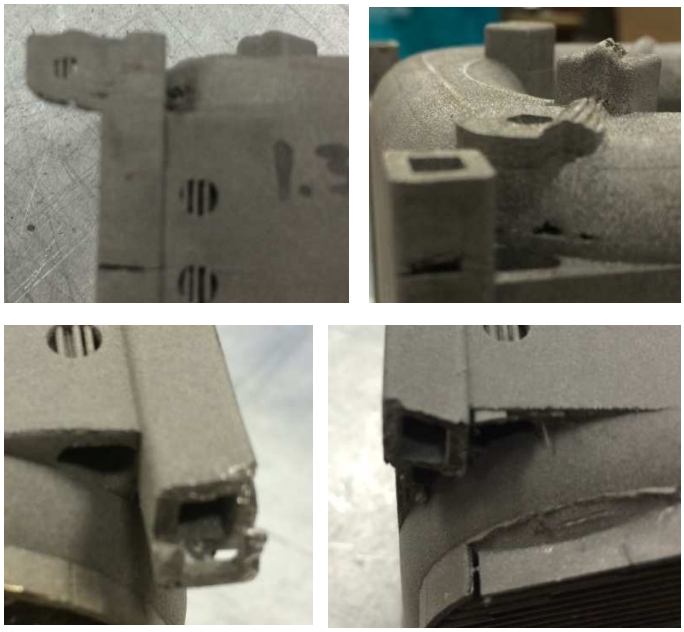

Figure 8: Laser sintering defects on the tank.

Electronics

Communication

The propulsion system was controlled via a GUI created in Python. The GUI communicated with an Arduino Micro 16MHz microcontroller, a 4 Input Phidget Temperature Sensor, and a 4 Input Phidget Bridge. These three circuit boards enabled readings from three pressure sensors (connected to the Arduino), four thermocouples (connected to the Phidget Temperature Sensor), one load cell (connected to the Phidget Bridge), and one scale (connected to the Arduino). Table 2 shows the approximate sampling frequency for each instrument.

Instrument	**Sampling Frequency (Hz)**
Pressure Sensor	375
Thermocouple	80
Load cell	125
Scale	3

Table 2: Sampling rate for each instrument.

The pressure sensors sent a 0-5V analog signal to the Arduino, which was then converted into a 10 bit number. The pressure sensors were calibrated up to 200 psi on test day. The thermocouples communicated with the Phidget Temperature Sensor, and the Phidget bridge was connected to a laptop via USB. The scale transfered data to the Arduino with serial communication. The Arduino was connected to the laptop with a USB cable. All of the circuit boards were on the test stand, and we used a Geffen USB extender to be able to communicate with the electronics from 150 ft away from the test stand.

Control

In addition to reading data from the pressure sensors and scale, the Arduino Micro controlled four solenoid valves and the glow plug igniter. The valve and igniter control were enabled by connecting the Arduino to two ET-OPTO RELAY-4 relay boards. This provided 12 Volts and sufficient current to power the solenoid valves and the igniter. The Arduino alone was not sufficient to power the valves and igniter because there was a 40 mA and 5 Volt limit for each I/O pin on the Arduino. By using the relay board, 12 Volt lead-acid batteries to powered the valves and igniter.

Problems were encountered when isolating the Arduino from the back EMF originating from the solenoid valves when the Arduino pins were connected directly to the relay boards. When the solenoid values were actuated, the Arduino would sometimes reset and stop communicating with the computer. This was fixed by using a KSP2222A transistor, a 10 kΩ resistor, and a 2 kΩ resistor for each pin to relay connection. The circuit for one pin to one relay board connection is shown in Figure 9.

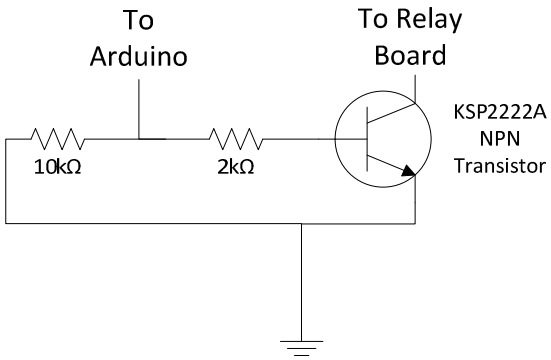

Figure 9: Circuit of Arduino pin connection to ET-OPTO relay board.

Safety

A hardware emergency stop system was used. When activated, the switch isolated the 12 Volt lead acid battery that powered the igniter, the fill valve, the upstream main valve, and the downstream main valve from the system. This enabled the purge and vent valves to remain open in the event of an emergency. Because of this necessary precaution, another 12 Volt lead acid battery was used to power the purge and vent valves.

Ignition

The ignition system of the SOURIS hybrid rocket was designed to provide sufficient thermal energy to start the combustion process in the thrust chamber. Although the initial goal was to design a high-current ignition system that would allow for multiple engine restart procedures in space, the team decided that a reliable, disposable pyrotechnic igniter would be more suitable for ground-test technology demonstration purposes.

The igniter consisted of an electrical McCoy-55 glow plug packed with a refined black powder variant and a small garolite tube containing a hollow pyrograin propellant for additional heat release. The pyrograin propellant was made of a mixture of finely grinded black powder and nitrous cellulose dissolved in acetone. Here, nitrous cellulose was used as a binding agent (upon vaporization of the

acetone) to constrain the propellant within the garolite tube, as well as to slightly reduce the burning rate of the pyrograin for a less strict ignition timing procedure.

Figure 10: McCoy-55 Glow Plug.

A 12V battery was used to activate the glow plug. Upon firing the igniter system, current flowed through a resistive coil (coated with magnesium oxide to protect the glow plug), heating the material and lighting up the black powder packed inside the glow plug. Hot gases produced by the glow plug would start the pyrograin and impinge on the tapered surface of the sold fuel grain, vaporizing a fraction of the PMMA fuel. Finally, the fuel vapor would mix with the nitrous oxide flowing through the injector orifice and, in the presence of the igniter flame, sustained combustion process in the chamber would initiate.

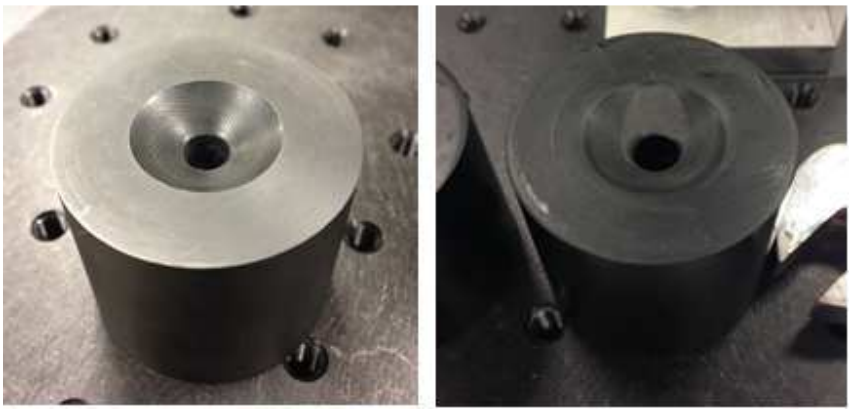

Figure 11: PMMA fuel grain a) before ignition test and b) after ignition test.

Given that ignition systems are particularly critical in any hybrid rocket engine, a significant amount of tests were carried in the laboratory to ensure that sufficient heat was being delivered to the fuel grain. These tests verified that the fuel combusted in the presence of atmospheric air and that the ignition system operated properly. Since pure nitrous oxide is a more reactive oxidizer than atmospheric oxygen, we were able to confirm igniter capability in a controlled environment prior to testing the rocket.

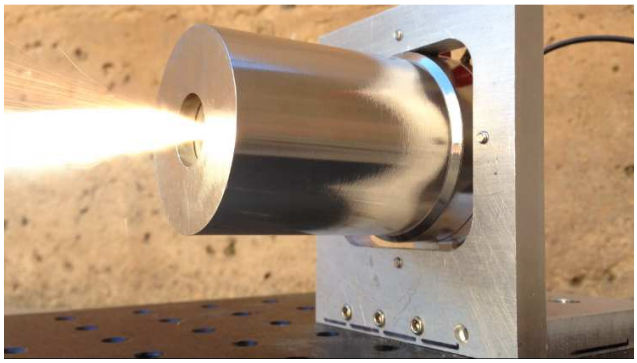

Figure 12: Ignition system test on fully assembled thrust chamber.

Hotfire Test Stand

Due to the size of the system, a self-contained mobile test stand was constructed to allow for multiple tests and easy transportation. The entire system is constrained on a two level cart. The upper level holds the 440 cm^3 oxidizer tank, main feedline and combustion chamber secured to a plate with c-clamps. This plate is supported on four thin metal strips to minimize dissipation to increase thrust measurement accuracy. Thrust is measured with a 10lbs load cell[3]. The entire system is placed on a scale to measure initial oxidizer mass and total mass flow. The lower level contains the electronic and measuring equipment.

A flashback arrestor[4] was introduced in the feedline to avoid any upstream propagation resulting in possible nitrous oxide decomposition hazards. Two main valves[5] were used for redundancy. The ground test facility contains a nitrogen purge system. Figure 13 shows the Piping and Instrumentation diagram for the ground test system.

[3] FUTEK LSB200

[4] SUPERFLASH Flashback Arrestor for Regulator and Point of Supply, Oxygen Service

[5] Parker S9 NC

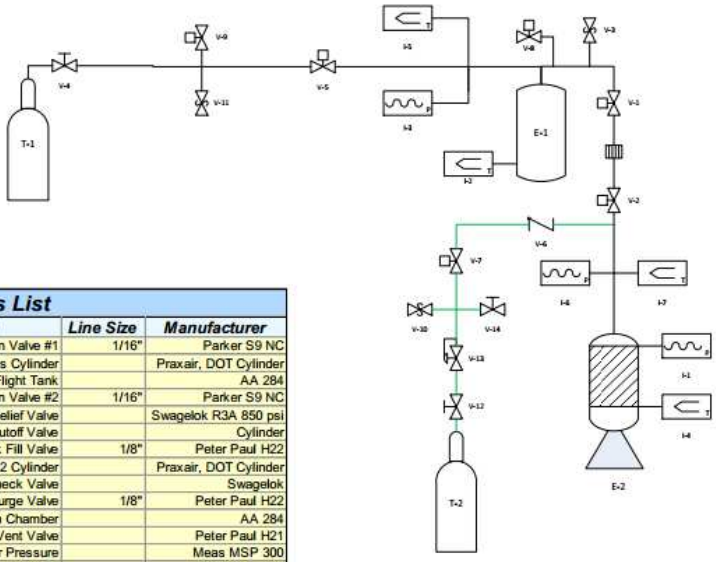

Parts List			
Displayed Text	**Description**	**Line Size**	**Manufacturer**
V-1	Main Valve #1	1/16"	Parker S9 NC
T-1	Nitrous Cylinder		Praxair, DOT Cylinder
E-1	Flight Tank		AA 284
V-2	Main Valve #2	1/16"	Parker S9 NC
V-3	Flight Tank Relief Valve		Swagelok R3A 850 psi
V-4	Nitrous Cylinder Shutoff Valve		Cylinder
V-5	Flight Tank Fill Valve	1/8"	Peter Paul H22
T-2	N2 Cylinder		Praxair, DOT Cylinder
V-6	N2 Purge Check Valve		Swagelok
V-7	Combustion Chamber Purge Valve	1/8"	Peter Paul H22
E-2	Combustion Chamber		AA 284
V-8	Flight Tank Vent Valve		Peter Paul H21
I-1	Combustion Chamber Pressure		Meas MSP 300
I-2	Flight Tank External TC		Omega, K type
I-3	Run Tank Pressure		Meas MSP 300
I-4	CC Throat External TC		Omega, K type
	Flame Arrester		Superflash
V-9	Nitrous Feedline Vent		Peter Paul H21
V-10	N2 Purge Relief Valve		Swagelok R3A 850 psi
V-11	Nitrous Feedline Relief		Swagelok R3A 850 psi
I-5	Nitrous Feedline TC		Omega, K type
I-6	Main Feedline Orifice Pressure		Meas MSP 300
I-7	Main Feedline Orifice TC		Omega, K type
V-12	Nitrogen Cylinder Shutoff Valve		Cylinder
V-13	N2 Regulator		

Figure 13: Ground test Piping and Instrumentation Diagram.

Pictures of the test article are shown below.

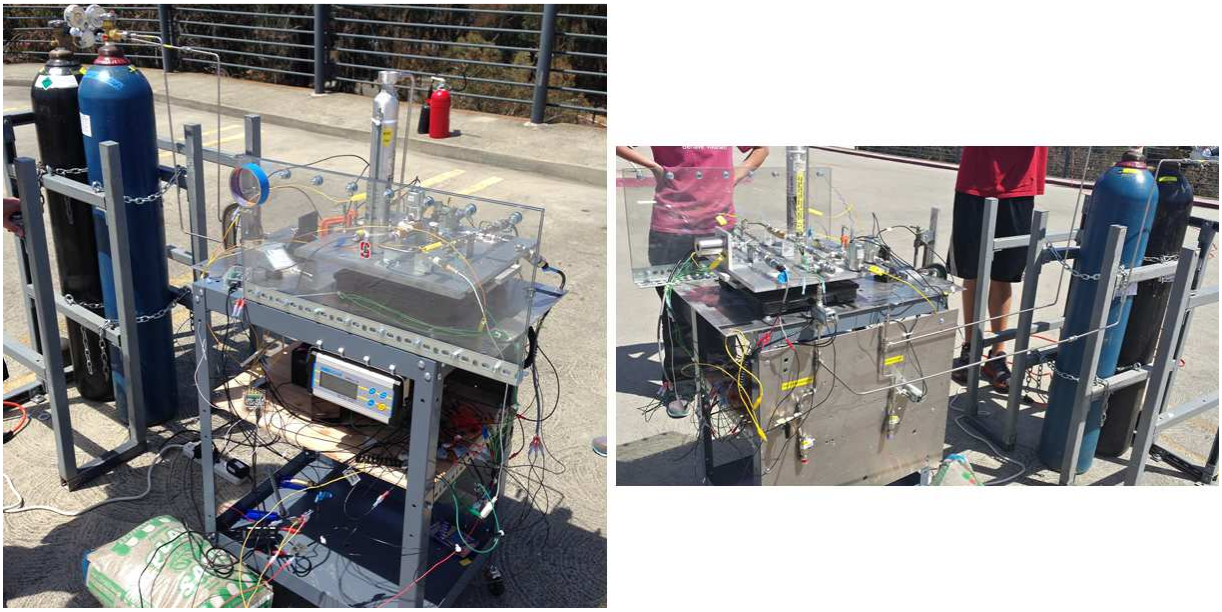

Figure 14: Test stand.

Test Day Proceedings

Testing of the ground system was performed on May 24th 2014 on the Stanford University campus. Multiple blowdown and cold flow tests were conducted before hot firing. Two successful rocket firings of 9.5 and 30 seconds were carried out.

On the first round of blowdown tests, it was discovered that the tank pressure transducer and the two stick-on thermocouples measuring tank temperature and chamber temperature produced flawed measurements. After some troubleshooting, it was determined that the transducer was working correctly, but had not been calibrated properly to read the expected tank pressures (a more thorough explanation is presented in the Error Analysis section). The problem with the thermocouples was determined to have been caused by improper installation. The sensing element to make contact with the metal installation surfaces and consequently become grounded. This problem could not be resolved with the given materials and time constraints on test day. As a result, these temperature readings were abandoned.

After performing cold flow tests with three different sonic orifice sizes, it was determined that both the oxidizer mass flow through the system and the pressure upstream of the orifice were lower than expected, due to much higher losses in the feedline. This presented a danger in the system as the much lower than predicted pressure upstream of the orifice would allow it to unchoke. Thus if spikes in chamber pressure were seen, a decomposition event in the feedline may have occured. To improve performance, the flashback arrestor was removed from the feedline. It was deemed the flow isolation across the sonic orifice would provide more safety against destructive decomposition events than an unchoked orifice and flashback arrestor. Further, the smallest 0.5mm orifice was selected for hotfire to ensure the orifice would choke properly. Both hotfires were performed without the flashback arrestor. As predicted, the SOURIS ignition system operated at a 100% success rate during test day, properly starting the rocket engine on both test runs.

In both of our hotfires, post-test analysis of the fuel grain showed significant erosion on the end, seen in Figure 15. It is hypothesized that a strong annular region of recirculating flow was created in the post combustion chamber due to the expansion in area upon exiting the port followed by the rapid decrease in area as the flow converged to the nozzle. This recirculation zone greatly improved mixing in the engine, leading to high c* and I_{sp} efficiencies seen during data analysis and lower O/F ratio than a simple regression model would predict. These effects were later observed in the data analysis. This recirculation zone would also provide flame-holding for the engine, helping it maintain combustion even at the lower extreme of oxidizer mass flux required to maintain a stable diffusion flame in the port.

Figure 15: Recirculation driven end burning in hotfires 1 (left) and 2 (right).

Data Analysis

Performance Parameters

Total average mass flow was calculated using the initial and final system mass and the burn time. Average fuel mass flow was calculated with initial and final mass of the PMMA fuel. Using these two values, the average oxidizer mass flow and O/F ratio can be calculated. Average values of thrust, total mass flow rate and chamber pressure can be used to determine specific impulse (I_{sp}) and characteristic velocity (c*). Instantaneous oxidizer mass flow was measured by flowing the oxidizer through a sonic orifice of known area, using the following equation.

$$\dot{m} = \frac{\gamma}{\left(\frac{\gamma+1}{2}\right)^{\frac{\gamma+1}{2(\gamma-1)}}} \left(\frac{P_t A}{\sqrt{\gamma R T_t}}\right)$$

Since the area ratio between the orifice and the tube area where the pressure and temperature were measured is greater than 5, the measured static pressure and temperature of the gas were assumed to be equal to the stagnation pressure and temperature at that point. Nitrous oxide has a compressibility factor close enough to 1 at the average pressure and temperature seen at the orifice, justifying the ideal gas assumption present in the equation above. The pressure ratio across the orifice was calculated to confirm that sonic conditions were present. For the second hotfire, the calculated average oxidizer mass flow rate gives a 12% error compared to the average value measured with the scale. This enables us to estimate the pressure dependency of the oxidizer mass flow rate. The thermoequilibrium code CEA gives us theoretical I_{sp} and c* to calculate efficiencies.

The pressure, scale and thrust time histories as well as performance parameters of interest for the two hotfires are shown in Figure 16 and Figure 17.

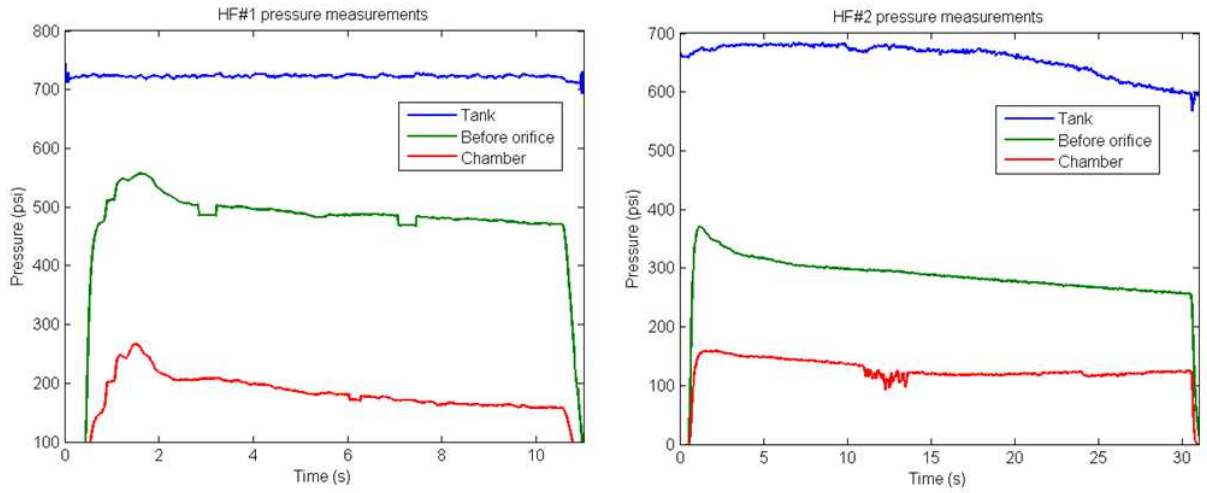

Figure 16: Pressure measurements for the two hotfires.

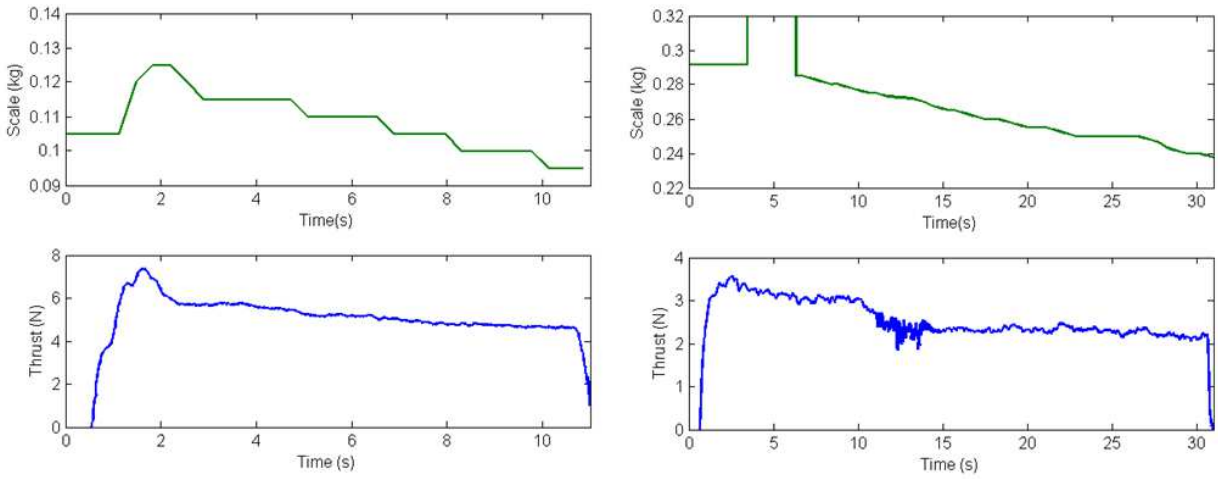

Figure 17: Scale and load cell measurements for the two hot fires.

	Hotfire #1	**Hotfire #2**	**Uncertainty (±)**
Burn time (s)	9.5	30	-
$\dot{m}_{tot}$ *(g/s)*	2.6	2	8%
$\dot{m}_f$ *(g/s)*	0.82	0.68	5 %
$\dot{m}_{ox}$ *(g/s)*	1.81	1.32	6 %
O/F ratio	2.05	1.94	0.14
Initial tank pressure (psi)	730	680	70 psi
Average chamber pressure (psi)	186	129	5 psi
Average feed line loss (psi)	230	370	70 psi
Average Thrust (N)	5.31	2.65	0.07 N
Max Thrust (N)	7.55	3.69	0.06 N

Average C (m/s)*	1,532	1,398	13 %
C efficiency*	102.2 %	115 %	14 %
I_{sp} *(s)*	206	135	8 %
I_{sp} *efficiency*	109.3 %	95 %	9 %
I_{tot} *(N.s)*	50.4	74	.6 N.s, 1.8 N.s

Table 3: Hotfire key performance metrics

Because the sampling frequency was fairly low, it was not possible to determine high frequency combustion instabilities, such as acoustic oscillations. A Fourier analysis of the chamber pressure for both firings showed very low frequency oscillations. Because these oscillations only occur during the burn, it can be determined that this frequency is unrelated to the sensor noise.

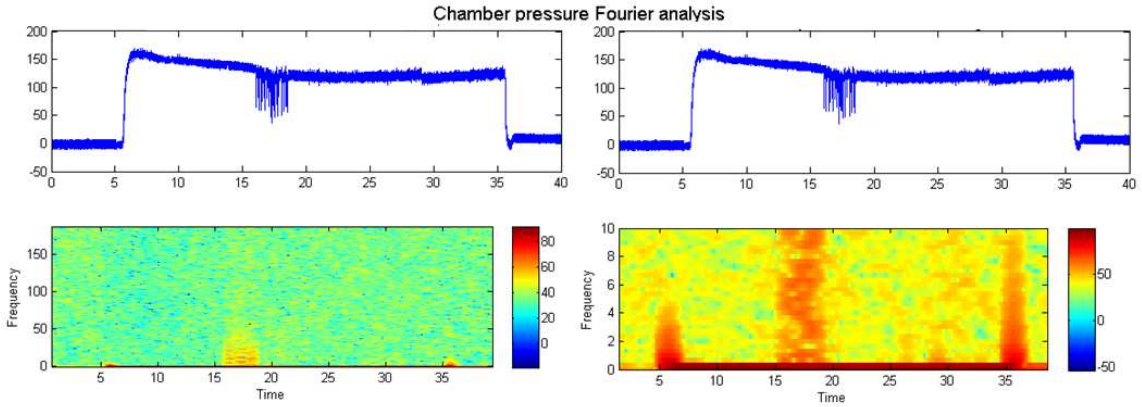

Figure 18: Fourier analysis for HF#2.

Error analysis

To get a sense of the uncertainty of the measurements, orifice and instrument tolerances and calibration fit uncertainties were collected for the pressure transducers, load cell, scale, and thermocouples. Since noisy measurements (such as pressure and load cell) were smoothed by moving average (as described above), the instantaneous mean uncertainty of the smoothed values was combined with the instrument uncertainty to obtain a total measurement uncertainty. Uncertainty propagation was used to determine the uncertainties of calculated engine parameters, as shown in the equations below. The uncertainties are recorded in Table 3.

$$\frac{\delta \dot{m}_{ox}}{\dot{m}_{ox}} = \sqrt{\left(\frac{\delta P_t}{P_t}\right)^2 + \left(\frac{\delta A_{orifice}}{A_{orifice}}\right)^2 + \left(\frac{\delta T_t}{2T_t}\right)^2}$$

$$\frac{\delta \dot{m}}{\dot{m}} = \sqrt{\left(\frac{\delta \dot{m}_{ox}}{\dot{m}_{ox}}\right)^2 + \left(\frac{\delta \dot{m}_{fuel}}{\dot{m}_{fuel}}\right)^2}$$

$$\frac{\delta c^*}{c^*} = \sqrt{\left(\frac{\delta P_{chamber}}{P_{chamber}}\right)^2 + \left(\frac{\delta A_{throat}}{A_{throat}}\right)^2 + \left(\frac{\delta \dot{m}}{\dot{m}}\right)^2}$$

The main sources of uncertainty and error are attributed to the pressure transducer on the tank, the orifice and nozzle throat, and the fuel mass flow estimation. The pressure transducer was only calibrated from 0 to 220 psi, corresponding to less than 10 % of the instrument range. Thus, the linear region of the instrument was not fully captured. Additionally, the expected tank pressures were 3x greater than the largest calibration point, introducing considerable uncertainty. This issue was partially solved by artificially adding a calibration point at the end of the transducer's range, assuming that at its maximum design pressure of 2500 psi it would output a full 5V signal. A more accurate solution would have been to buy a higher pressure regulator and calibrate the transducer in 100 or 200 psi increments from 0 to 1000 psi.

Both the orifice and the nozzle throat were not calibrated against a known orifice, so their uncertainties had to be calculated from the manufacturer stated tolerance on diameter. The fuel mass flow rate cannot be measured directly, and was assumed to be constant as determined by the initial and final fuel grain mass. Time histories of the oxidizer mass flow and observation of the fuel grain regression pattern show this is highly unlikely, leading to uncertainty.

Lastly, the oxidizer mass flow calculation assumed that the oxidizer is an ideal gas. The compressibility factor of the oxidizer right before the orifice is 0.84 for the second hotfire, and a calculation using real gas properties from REFPROP shows it would stay gaseous with the same compressibility at mach 1 through the orifice. On the other hand, the oxidizer has a compressibility factor of 0.73 for the first hotfire, and would partially condense before accelerating to mach 1. These real gas effects add uncertainty to the mass flow measurement which is difficult to quantify.

Modeling Comparison

When comparing the test measurements with the design time histories obtained by simulation and presented in Figure 6, the actual performance of the engine appears to be much lower than expected. This is due to the fact that feed line pressures losses were underestimated (only 100 psi was anticipated), and the oxidizer mass flow rate was less than half the mass flow rate predicted by simulation. The superposed time histories are shown below for the 30s hotfire.

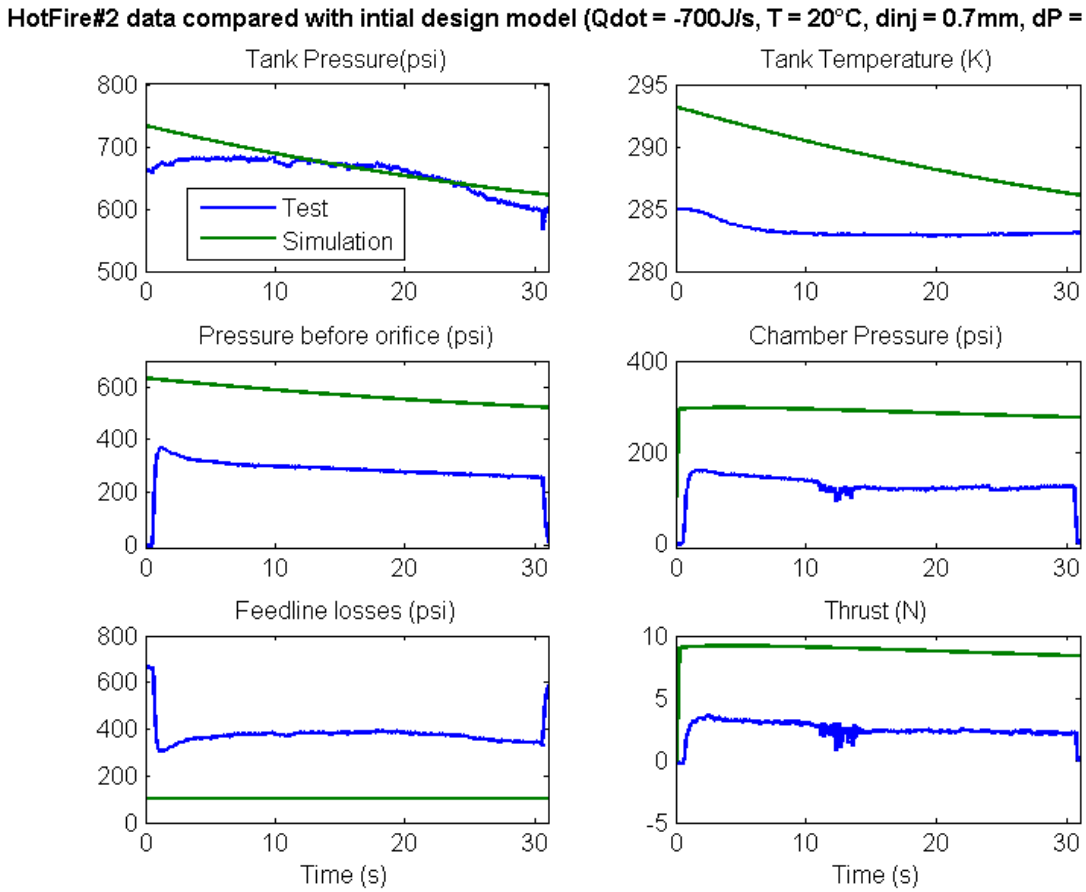

Figure 19: 30s hotfire measurements compared to design modeling.

Nevertheless, knowing the feedline losses between the tank and the orifice pressure measurements, we can include the test value in the simulation to determine the accuracy of the modeling. First, the regression simulation was tested and then the complete code. Using the calculated oxidizer mass flow, the regression rate of the fuel can be determined, enabling us to estimate the total mass flow and the oxidizer to fuel ratio. Engine performance can be simulated using CEA. The results are shown below for the 30s hotfire.

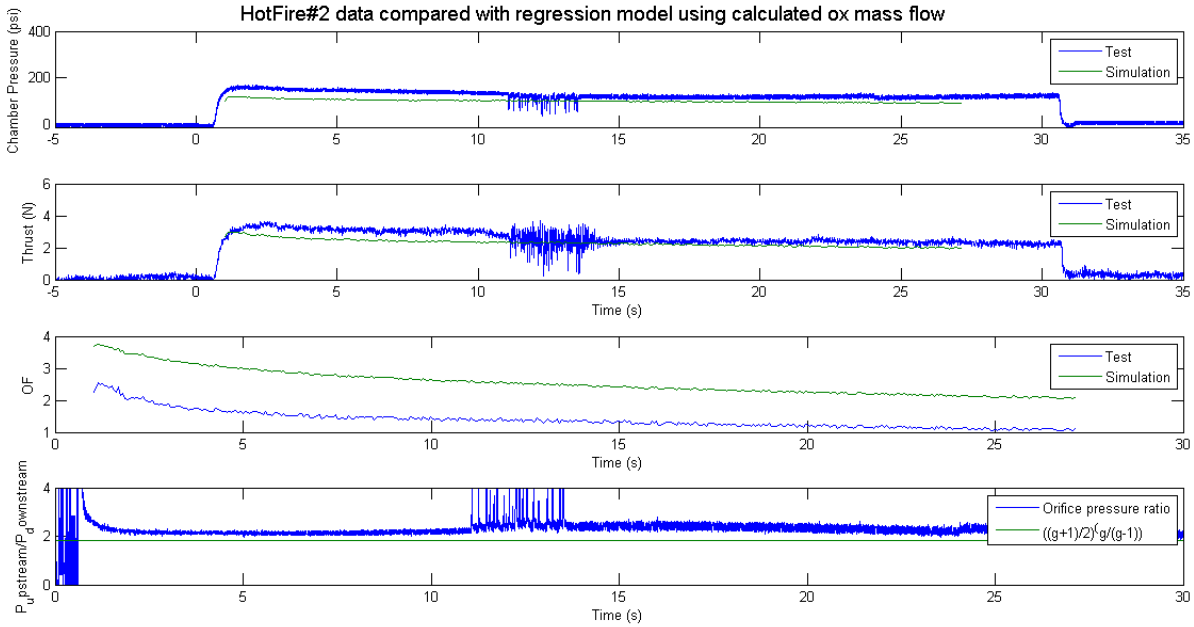

Figure 20: 30s hotfire measurements compared to regression rate model

The last plot ensures that the orifice is always sonic. The O/F ratio versus time shows that the regression model overestimates the oxidizer to fuel ratio. This means that the model underestimates the fuel regression and so the fuel mass flow rate. In fact, the model estimates the final mass of burned fuel to be 11.95 g. The measured mass of burned PMMA for this test was 20.4 g. This shows the limits of the regression model used, which assumes a constant port opening. As a matter of fact, the fuel grain showed a strong recirculation zone at the aft end, shown in Figure 15, resulting in quasi complete burn. As seen on the first two plots, chamber pressure and thrust can are estimated with an average error of 21% and 14%, respectively.

By integrating the regression model in the complete code simulating the blowdown of the tank with the feed line pressure loss as an input, the following results were computed for the 30 s burn:

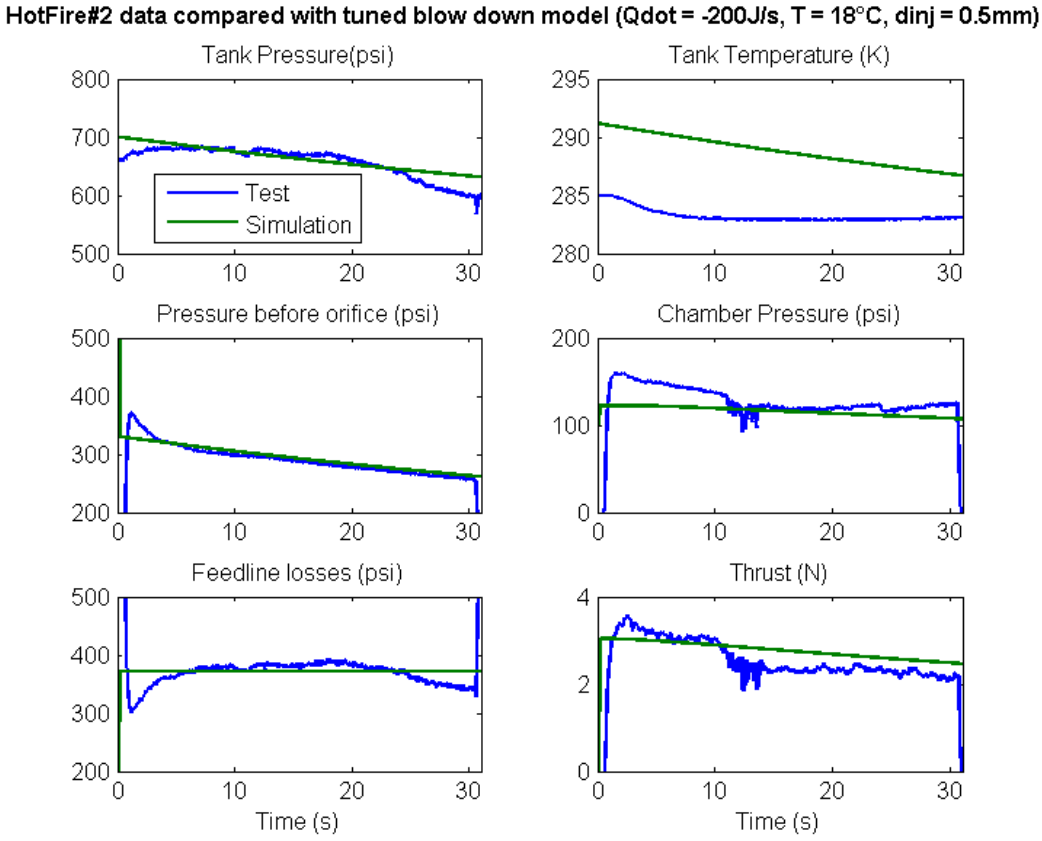

Figure 21: 30s hotfire compared to complete model results

The heat transfer rate was iteratively defined in order to adjust the temperature drop in the tank to reasonable values and was determined to be about -200 J/s. Note that the slope of the curve for the pressure upstream of the orifice seems well caught. The average chamber pressure is estimated with a 13% error and the average thrust with an error of 0.75%. More tests would need to be conducted to conclude on the accuracy and robustness of the developed model.

Conclusion

In this project a hybrid propulsion system for CubeSat using Nitrous Oxide and PMMA was designed, manufactured and tested. The combustion chamber is nested in a toroidal oxidizer tank. The assembled system without main feed line or electronic components fits within a one unit (10x10x10 cm). Because the 3D printed titanium tank presented laser sintering defects, it did not hold the required pressure. A substitute tank of similar volume was used for testing the system. Two hotfires of 9.5 and 30 seconds using an orifice of 0.5mm were demonstrated on May 24th 2014. Feed line pressure losses were considerable, significantly decreasing the oxidizer mass flow rate, thus the total mass flow rate and so the engine performance. The average thrust for the short duration burn was 5.31N and 2.65N for the long duration burn. Calculated average I_{sp} were respectively 206s and 135s. The low accuracy of these measurements result in non-negligible uncertainties.

A 3D printed stainless steel oxidizer tank is to be pressure tested in the near future. Possible modifications to the system would involve replacing the two main valves by bigger valves, shortening the feed line, reducing the number of fittings and connections in order to reduce the pressure losses between the tank and the orifice in order to achieve higher performance and meet the set requirements. The tank pressure transducer would be replaced by a sensor rated to a more suited range and calibration would be done on the final system with higher pressures. Stick on temperature sensors would be placed and tested on the tank and chamber. Ideally, temperature and pressure would be measured in the tank and not in the feed line and all measurements would be recorded with a higher sampling frequency in order to determine combustion instabilities.

Acknowledgements

The 2013-2014 AA284 class would like to thank the King Abdulaziz City for Science and Technology (KACST) for funding this work. We would like to thank B. Evans, B. Jens, P. Narsai, J. Stober, B. Waxman, J. Zimmerman from the Stanford Propulsion and Space Exploration Group and Professor Brian Cantwell for their valuable input during the reviews and their help in the lab. Finally, the SOURIS team would like to thank G. Zilliac from NASA Ames for admirably creating an autonomous learning environment, leading to a valuable and enriching experience.